Journal of Engineering Technology and Applied Physics

Comparison Study of Natural Dye Sensitisers in Dye-Sensitised Solar Cells

Faisal Abdullah Sadeq[1], Cheikh Zakaria Eldjilali[1], Pei Ling Low[1, 2], Gregory Soon How Thien[2], Kar Ban Tan[3], H. C. Ananda Murthy[4], Muhammad Aqeel Ashraf[1], Kah Yoong Chan[1, 2, *]

[1]*Faculty of Artificial Intelligence and Engineering, Multimedia University, Persiaran Multimedia, 63100 Cyberjaya, Selangor, Malaysia.*

[2]*Centre for Advanced Devices and Systems, COE for Robotics and Sensing Technologies, Multimedia University, Persiaran Multimedia, 63100 Cyberjaya, Selangor, Malaysia.*

[3]*Department of Chemistry, Faculty of Science, Universiti Putra Malaysia, 43400 Serdang, Selangor, Malaysia.*

[4]*Department of Applied Sciences, Papua New Guinea University of Technology, Lae, Morobe Province, 411, Papua New Guinea.*

**Corresponding author*: kychan@mmu.edu.my, *ORCiD*: 0000-0003-1076-5034

https://doi.org/10.33093/jetap.2025.7.2.3

Manuscript Received: 9 April 2025, Accepted: 23 May 2025, Published: 15 September 2025

***Abstract* — This work explored the performance and characterisation of dye-sensitised solar cells (DSSCs) based on sustainable dyes, as compared to traditionally applied dyes consisting of metal compounds. Several natural sources were used to extract the dye, including mangosteen, thyme, coriander, spearmint, ginger, and papaya. The samples were investigated, and a comparison was made between the performance of each dye. The ruthenium sensitised control sample yielded a Power Conversion Efficiency (PCE) of 3.9642% with a Fill Factor (FF) of 69.434%. Among natural dye sensitisers anthocyanin pigment-rich dye from mangosteen performed the best with PCE and FF of 0.7677% and 68.55%, respectively. Other natural dye-sensitised samples all depicted PCE < 0.3% but relatively close FF, ranging from 50% to around 70%.**

***Keywords*—Solar Cells, Photovoltaics, TiO_2, DSSC, Anthocyanin, Chlorophyll, Natural dye.**

I. INTRODUCTION

The Earth's climate is a growing concern, with rising temperatures, ozone layer depletion, and an increase in carbon dioxide (CO_2) and other greenhouse gas emissions causing alarm worldwide. Global CO_2 emissions in 2022 rose by 0.9% to a new all-time high of 36.8 gigatons [1]. Two new ozone holes formed in the last 5 years. The hole formed in 2019 had been short-lived; however, the 2022 ozone layer hole has been persistent and larger in size than the average over the last 10 years [2 - 4]. According to the 2024 Global Climate Report from NCEI, or National Centres for Environmental Information, 2024 was recorded to be the warmest year, with 1.29 ℃ above the 20th century average temperature [5]. Frequent flooding around the world in the past months because of rising sea levels are proof of the impending danger that awaits if the world fails to act on it. These changes, coupled with the ever-increasing demand for electricity, have prompted a surge in research and development of renewable energy sources.

With the aim to battle climate change in mind, solar energy has gained significant traction globally in recent years as a prominent source for renewable energy [6]. Various technologies have been invented to harness solar radiation energy, such as photovoltaic/thermal (PV/T) that convert both thermal and electrical solar energy, or photovoltaic (PV) only solar cells [7]. The continuous development of PV has given rise to various types of solar technologies, such as monocrystalline silicon, organic polymer solar cells, perovskite solar cells, or dye-sensitised solar cells [8 - 11]. Among these, DSSCs have emerged as a promising alternative due to their lower production costs, and relative stability. On grounds of having a relatively low manufacturing cost, size and ease of use, PV has been a popular choice for renewable energy generation, especially in specific applications like agriculture, streetlamps and (flood) detection systems [12, 13].

Dye-sensitised solar cells (DSSCs) are a 3rd generation photovoltaic technology that has gained significant attention since their introduction by Michael Grätzel and Brian O'Regan in 1991 [14]. Unlike conventional silicon-based solar cells, DSSCs

rely on a photoactive dye to absorb sunlight and generate electricity through a process that mimics natural photosynthesis. This technology offers several advantages, including relatively low production costs, flexibility, and the potential for semi-transparency, making it suitable for a wide range of applications, such as building-integrated photovoltaics and portable devices.

The core components of a DSSC include a photoanode, typically composed of a mesoporous titanium dioxide (TiO_2) layer which performs as the electron transfer layer, a sensitising dye for photogeneration, an electrolyte containing a redox couple, and a counter electrode. The operation of a DSSC involves the absorption of photons by the dye, which results in the excitation of electrons. Electrons are excited from the highest occupied molecular orbital (HOMO) in the ground state to the lowest unoccupied molecular orbital (LUMO) [15]. These electrons are then injected into the conduction band of the TiO_2 and transported to the external circuit to generate electrical power. The oxidised dye molecules are subsequently regenerated by the redox couple in the electrolyte, which completes the electrical circuit by donating electrons from the counter electrode [16].

DSSCs present several key advantages over traditional silicon-based photovoltaic cells. One of the most significant benefits is their lower production cost. The materials used in DSSCs, such as TiO_2 and the various organic or inorganic dyes, are less expensive and require less energy-intensive manufacturing processes compared to silicon. Additionally, DSSCs can be fabricated on flexible substrates [9], allowing for innovative applications, including flexible solar panels and semi-transparent devices that can be integrated into windows and other architectural elements.

The dye characteristics play a crucial role in the absorption of light. In theory, an efficient dye should be able to absorb the visible and near-infrared light with high electron mobility. There are two categories of dyes in literature: metal-based dyes and metal-free organic dyes. Even though metal-based DSSCs have a lot of advantages to them, they are still plagued by high material fabrication costs and low efficiencies, which have prevented DSSCs from getting commercialised [17]. The best-performing DSSCs utilise metal compound synthetic dyes, like ruthenium (Ru)-based dyes, as sensitisers. These dyes are often costly due to their intricate synthesis processes, the scarcity of noble metals, and sometimes due to the difficulty in handling metals that are toxic in nature. It has been a long-running effort to transition to more sustainable materials and processes for DSSC fabrication.

Various organic materials have been investigated in DSSCs to reduce fabrication costs, improve efficiencies and enhance durability. Polymer organic materials and carbonaceous materials have been used in the development of photoanodes. While other light-sensitive organic and natural dyes are broadly designed to achieve high power conversion efficiencies [17].

Due to the exceptional performance of DSSC in artificial/indoor light, they offer promise in indoor applications like self-powered indoor IoT sensors and devices [17]. Furthermore, due to their simplicity, fabrication cost, and aesthetic value, DSSC are more desirable in building integrated designs or building integrated photovoltaics (BPIV) [18, 19]. Green dye-based DSSCs mean there is an assortment of colours to choose from.

Green-based dyes in DSSCs have started gaining traction again in recent years as the world starts to move towards more sustainable processes in manufacturing. While the PCE of green-based dyes is relatively low, the vast availability of the green materials makes it an attractive research topic for solar cells. There exist several plants and fruits that can be implemented for light absorption. Mangosteen (Garcinia mangostana L.) fruit is famous in South Asia for its purple rind colour and its unique taste. Mangosteen rind is rich primarily with anthocyanin pigments [20]. Chlorophyll a, b, and carotenoid pigments are found in many green plants, as they play a vital role in the photosynthesis process. Thyme (Thymus vulgaris L.), spearmint (Mentha spicata L.), and coriander (Coriandrum sativum L.) contain high concentrations of chlorophyll and carotenoid pigment in varying amounts [21 - 23].

Antioxidant-rich fruits such as ginger (Zingiber officinale Roscoe) are famous for their pale-yellow colour, which can be attributed to the presence of curcumin pigment [24, 25]. Papaya (Carica papaya L.) also contains a high amount of antioxidant compounds, such as β-carotene pigments [24, 25].

This work explores the performance and characterisation of DSSCs based on sustainable natural dyes as compared to more traditionally applied dyes consisting of metal compounds. The extraction methods for dyes from several different natural sources, such as mangosteen, thyme, spearmint, coriander, ginger, and papaya, were investigated, and a comparison was drawn between the photovoltaic performance and the absorption and transmittance spectrum of each different dye. The best-performing natural dye was investigated in comparison to the commercial Ru-based dye sample using electrochemical impedance spectroscopy (EIS).

II. EXPERIMENTATION AND METHODOLOGY

The paper investigated six different natural dye sources: mangosteen fruits, fresh thyme, coriander leaves, spearmint, papaya, and ginger. Dyes were extracted from each of the sources, and individual samples of DSSC were produced, each based on a different extracted dye. A separate sample using ruthenium-based dye was produced as the control sample for the study.

Table I. Label assignment to different samples.

No	Sample	Label	Details
1	Ruthenizer 535-bisTBA (N719)	Ru	For ruthenium based commercial dye (Solaronix)
2	Mangosteen	M	For dye extracted from mangosteen fruit pericarps
3	Thyme	T	For dye extracted from fresh thyme leaves and stems
4	Coriander	C	For dye extracted from fresh coriander leaves and stems
5	Spearmint	S	For dye extracted from fresh spearmint leaves and stems
6	Ginger	G	For dye extracted from ginger peels and flesh
7	Papaya	P	For dye extracted from papaya peels

A. Sample Labelling

Moving forward, samples are referred to by their respective labels for easy organisation and representation of data. Table 1 displays details of samples based on the extracted dyes and their respective labels.

B. Dye Preparation: Preparation of Synthetic (Commercial) Dye

The dye solution was prepared using 5.00×10^{-3} M of Chenodeoxycholic acid (CDCA) (Solaronix) and 5.00×10^{-4} M of ruthenium-based N719 dye, Ruthenizer 535-bisTBA (Solaronix) [26]. The procedure and methods were as reported by Yeoh *et al.* 2017 [28]. The solvents were dissolved in ethanol and mixed thoroughly in an ultrasonic bath to produce the dye solution.

C. Dye Preparation: Extraction from Thyme, Spearmint & Coriander

The dye extraction process, for all leafy greens and herbs, was similar. 1.25 g of leaves were measured out and crushed using mortar and pestle. The crushed samples were added to a beaker containing 25 ml of ethanol. The beaker was covered with parafilm and stirred on heat (using a magnetic stirrer) at 60 degrees Celsius for 30 minutes. After taking the mixture off the heat and allowing it to cool for 5 minutes, the mixture was then filtered to get the dye solution. All samples were procured from local groceries and vegetable stands.

D. Dye Preparation: Extraction from Mangosteen

Fresh mangosteen samples were sourced from nearby fruit vendors and neighbourhood grocery outlets. Extraction of dye from mangosteen fruits began with processing of the fruit peels. The pericarps of the fruit were separated from the white flesh of the fruit, refrigerated, cut into pieces, and finally pulsed into a powder using a blender. To have an even consistency and grain size, the powder was passed through fine-wire mesh. The powder was measured out and added to a beaker containing 25 ml of ethanol. The mixture was then stirred on heat for 30 minutes before filtering out the dye solution.

E. Dye Preparation: Extraction from Ginger

Ginger was cut into small pieces, without removing the skin, measured out and crushed slightly using a mortar and pestle. The crushed sample was added to an ethanol solution and stirred on heat before cooling and filtering to get the dye solution. The ginger used in this study was acquired from local markets and traditional vegetable stalls.

F. Dye Preparation: Extraction from Papaya

Ripe papayas were obtained from local produce stands and commonly frequented supermarkets. Dye was extracted from papaya peels by cutting the peels into small pieces and immersing them in ethanol. The sample + ethanol mixture was then stirred and filtered, resulting in the dye solution.

G. Standard Operating Procedures

Some standardisations were made for the extraction processes of dye for the different samples in order to reduce the number of variations in the experiment. For the dye extractions, ethanol was used as the solvent, and the volume was fixed at 25 ml. 1.25 g of solute was always used in the above processes. All mixtures were stirred using magnetic stirrer, with stirring time set at 30 minutes and stirring temperature of 60°C. After stirring, all the mixtures were filtered using Abet (520) filter paper to get the final dye solutions.

H. DSSC Fabrication

The working electrode was prepared by masking a cleaned fluorine-doped tin oxide (FTO) coated glass (sheet resistance 15 Ω/sq, transmission > 80% in the visible, dimension 20mm×20mm, thickness 1.6mm) sourced from Han Xin Industry Co. Ltd., Shanghai, China, with 3M Scotch tape. TiO_2 nanoparticle (Solaronix paste, Ti-Nanoxide D) layer was deposited using the doctor blade method onto the masked FTO

glass. The glass with TiO_2 deposit is sintered on a hotplate at 450℃ for 30 mins to remove organic solvent present in the TiO_2 paste and crystalize the TiO_2 to anatase form [27]. After the sintered samples are cooled down, the samples are immersed in the separate dye solutions prepared beforehand, with the active site facing up to ensure proper absorbance of the dye. The samples are immersed in the dye solutions for 12 hours to ensure adequate adsorption. A separate FTO glass is prepared for the counter electrode. The glass is masked and deposited with Platisol T/SP (Solaronix) by the doctor blade technique. To activate the platinum layer, the platinised glass was sintered at 450℃ for 30 mins.

DSSC performance is governed by multiple factors, including the morphology and structure of photoanode. Photoanode thickness optimisation is one parameter that can lead to improved efficiency. As reported by Yeoh *et al.* from past measurements conducted in our labs, 4μm is the optimised thickness of TiO_2 layer for the best performance [28]. The same techniques and TiO_2 thickness reported were used in this study.

The device is completed by sandwiching the working electrode and counter electrode together, offset at either end along the length of the electrodes to provide space for probing. Iodolyte AN-50 (Solaronix) electrolyte was applied to the device between the electrodes via capillary action. Figure 1 shows the exploded view of a typical DSSC, highlighting the different layers present in its structure. Only one type of electrolyte was used to avoid having multiple variables in the experiment and to make sure only the performance of the dye layer is assessed. Iodide/triiodide electrolyte was specifically used due to its reported use in some of the most efficient DSSCs, as well as the I^-/I_3^- redox couple offering fast regeneration of the dye molecules and low recombination losses [29].

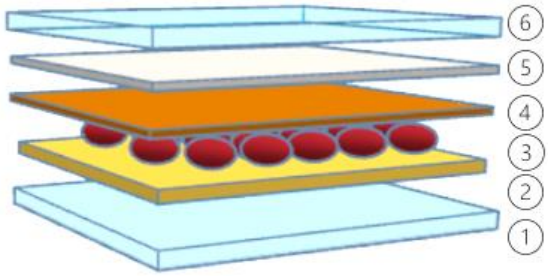

Fig. 1. DSSC exploded view (1 – FTO working electrode, 2 – mesoporous TiO_2 layer, 3 –dye molecules, 4 – electrolyte layer, 5 – platinum catalyst layer, 6 – FTO counter electrode).

I. Testing and Characterisation Methods

Photovoltaic performance of the DSSC samples was measured using the Oriel Sol2A Solar Simulator (Model No.6255, Oriel) utilising a 150W xenon lamp. The calibration of the simulated solar power was set at 100 $MWcm^2$, corresponding to standard air mass 1.5 solar conditions, using the Oriel PV reference cell system (Model 91150 V). The photocurrent-voltage characteristics were obtained by applying a bias to the sample cell(s) and measuring the resultant current with the Keithley Series 2400 Source Meter. The data of solar simulation was obtained from Oriel I-V Test Station software. Equations (1) and (2) represent the relation of FF and PCE (η) with current density (J) and voltage (V), respectively. This relation is used to compute parameters like FF and PCE from J – V (or I – V) characteristics.

$$FF(\%) = \frac{J_{max} \cdot V_{max}}{J_{SC} \cdot V_{OC}} \times 100 \quad (1)$$

$$\eta(\%) = \frac{J_{max} \cdot V_{max}}{P_{in}} \times 100\% \quad (2)$$

Ultraviolet-visible spectroscopy (UV-Vis) was conducted using an Avantes AvaSpec-ULS3648 spectrometer paired with an AvaLight-DHc light source from Avantes to measure the absorbance and transmittance characteristics of the cells. The Gamry Interface 1010E Potentiostat was utilised to make Electronic Impedance Spectroscopy (EIS) measurements at ranges of 0 – 100 MHz frequencies for the readings. X-ray diffraction spectroscopy (XRD) and field emission scanning electron microscopy (FESM) were carried out to verify the crystal structure and morphology of TiO_2 on FTO glass. FESEM images were processed using ImageJ software to study the porosity of the TiO_2 thin film [30].

III. RESULTS AND DISCUSSIONS

Figures 2 and 3 show the XRD spectroscopy and FESM image for TiO_2 film on FTO glass, respectively. The high-intensity peak at 25.29 degrees represents the (1 0 1) plane in the crystalline structure, while the comparably lower peak at 37.77 degrees represents the (0 0 4) plane. The two peaks confirm that the sample is a pure TiO_2 anatase crystal structure, with the absence of rutile peaks. As can be seen from a comparison to past papers and the JCPDS Card (no. 21-1272) [31], this is the expected spectra for nanoparticle TiO_2 film [32].

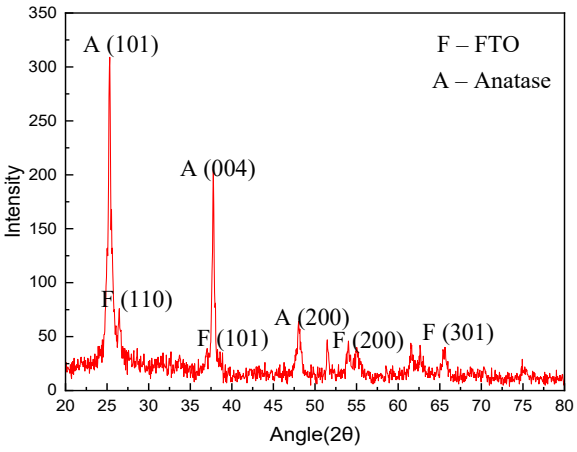

Fig. 2. XRD characterisation of TiO_2 on FTO.

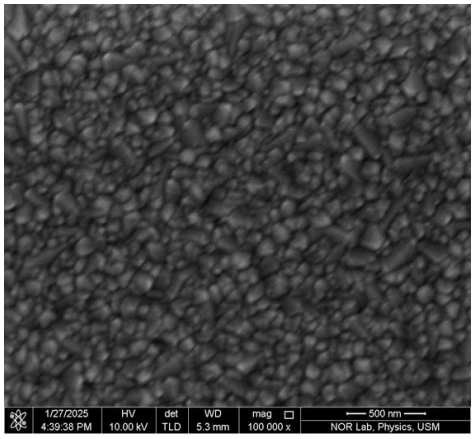

Fig. 3. FESEM for TiO_2 film on FTO glass.

The FESM results in Fig. 3 show the surface morphology as tightly packed particles in the crystalline structure, continuous and homogenous without cracks or blemishes. This shows the formation of aggregated TiO_2 nanostructures.

The pore sizes and overall porosity were extracted from the FESEM image using ImageJ software. The surface porosity was shown to be 3.424%. The individual area of pores was converted to equivalent diameter using the given Eq. (3) [33]. The average pore size was found to be 5.884 nm with a standard deviation of 7.329 nm.

$$d = 2 \times \sqrt{\frac{Area}{\pi}} \quad (3)$$

Table II summarises the photovoltaic parameters of DSSCs sensitised with different dyes. From Table II, the reported V_{OC} for sample Ru is 715.88 mV with a short-circuit current density (J_{SC}) of 7.9752 mA/cm^2. Resulting in Ru having the highest comparative PCE and FF among all the samples. With a V_{OC} of 636.85 mV and J_{SC} of 1.7584 mA/cm^2, sample M performed the second best overall. Samples T, C, S, G and P performed poorly with very low photocurrent generation (I_{SC}). Sample T observed the lowest open-circuit voltage (V_{OC}) and I_{SC} across the reading.

Table II. Photovoltaic parameters of DSSC based on different dye.

Sample	V_{OC} (mV)	J_{SC} (mA/cm^2)	I_{SC} (mA)	V_{OC}_Max (mV)	I_{SC}_Max (mA/cm^2)	Pmax (mW)	PCE (%)	FF (%)
Ru	715.88	7.9752	11.963	556.16	10.692	5.9463	3.9642	69.434
M	636.85	1.7584	2.6376	491.73	2.3417	1.1515	0.7677	68.552
C	632.04	0.82920	1.24381	417.91	0.94896	0.39657	0.2644	50.446
S	593.66	0.32423	0.48635	465.78	0.38525	0.17944	0.1196	62.150
G	554.46	0.35190	0.52786	420.63	0.42895	0.18043	0.1203	61.6483
P	521.08	0.24935	0.34091	378.33	0.29889	0.11308	0.0754	58.0193
T	476.04	0.11098	0.16647	338.26	0.12722	0.043033	0.0287	54.305

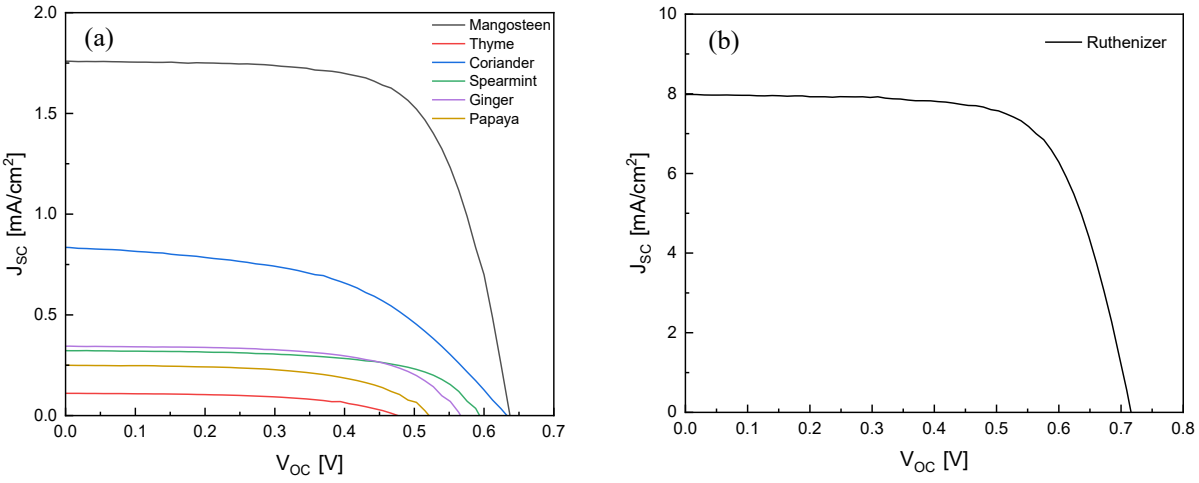

Fig. 4. (a) J – V characteristics curve of DSSCs based on different natural dyes, (b) J – V characteristics curve for Ruthenizer based DSSC.

The control sample, Ru, showed a better performance, likely due to the superior light harvesting properties, the reason for which lies in the metal-ligand charge transfer (MLCT) transition [34]. Among green dyes used as sensitisers, sample M performed the best. Sample M being sensitised using extraction of mangosteen fruit rind, contained anthocyanin pigments, which seem to work better in photogeneration of current compared to dyes based on chlorophyll pigment [35, 36]. Figure 4 displays the J-V characteristics comparison of the samples. The key difference highlighted between well-performing

samples and poorly performed ones is the large deviation in their photocurrent. For the best-performing sample, Ru, the I_{SC} was 11.963 mA. Among the better-performing natural sensitisers, sample M showed an I_{SC} of 2.64 mA and sample C demonstrated a 1.24 mA short-circuit current, while all other samples yielded $I_{SC} < 1$ mA.

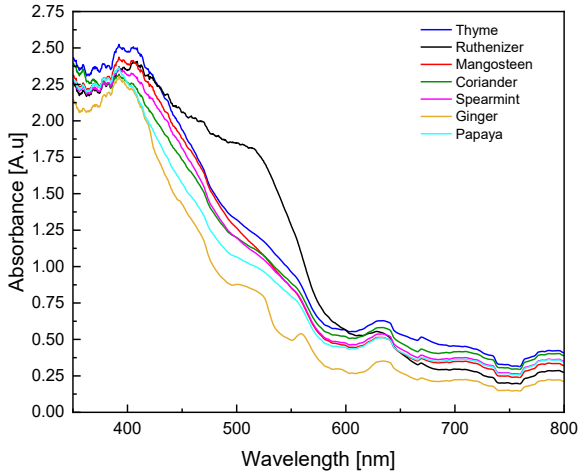

Fig. 5. Absorption spectra of tested DSSC samples.

Figure 5 shows the optical absorbance of the different devices (samples). The measurements were taken in the range of 350 – 800 nanometres (nm) wavelength. Among the dyes tested, T exhibits the highest absorbance peak, particularly in the 400–550 nm range, while sample Ru shows a wider spectrum compared to other dye samples. Light/photon absorption by dye is crucial for efficient light harvesting in DSSCs. All the dyes, while showing varying degrees of absorption, follow a similar trend, with absorption decreasing towards the near-infrared region (> 700 nm). This decline suggests that these dyes primarily capture visible light and may not efficiently utilise longer wavelengths. Hence, the study focused on the absorbance in the near-visible spectra for all dye samples.

Each TiO_2 photoanode was treated using the same procedure: identical dye volumes, a soaking time of 12 hours, and a film thickness of approximately 4 µm. This consistency made it possible to compare how much dye each film retained. To observe this, absorbance spectra were collected using UV-Vis, providing insight into the interaction between different natural extracts and the TiO_2 layer.

Figure 6 illustrates the transmittance spectra of DSSCs sensitised with different dyes. Higher transmittance values suggest lower light absorption, meaning that a significant portion of the incident light is passing through the material rather than being captured for energy conversion. Among the tested dyes, G exhibits the highest transmittance, particularly in the 650–800 nm range, indicating weaker absorption in this region. In contrast, Ru and other dyes demonstrate lower transmittance, suggesting better light-harvesting efficiency in the visible range. In the 350 – 650 nm range, Ru has the widest low transmittance width in the visible range. This corresponds to the high absorbance by Ru in the same range.

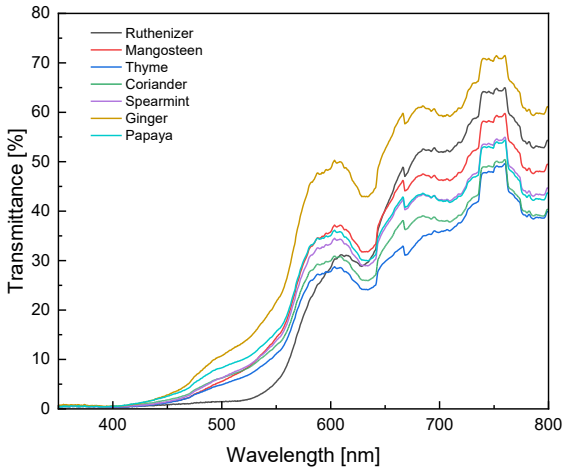

Fig. 6. Transmittance spectra of tested DSSC samples.

J. Equations

By comparing Figs. 5 and 6, it is evident that dyes with lower transmittance in key spectral regions exhibit higher absorbance, which is crucial for DSSC performance.

Observing the photovoltaic data, sample M depicts better Voc, Isc, and PCE in comparison to all different natural dyes evaluated. Anthocyanin is present in mangosteen while absent in all different natural dyes that have been tested [36]. It is suggested that the presence of the anthocyanin in the natural dye can boost the photovoltaic performance of the DSSC sample.

T, C, and S contain chlorophyll pigments, and so these can be sorted and compared as one class. Solar simulator results, V_{OC}, I_{SC}, and PCE show that C values are the highest, followed by S values and then T values. From the absorption spectrum, Fig. 5, the T peak has the widest range, followed by S and C in the respective class. The same is observed for absorption peaks, where in this class T had the highest peak, followed by S and C. Therefore, it can be inferred that for this class of samples that is rich with chlorophyll pigment, an inverse correlation is observed between absorption peak, spectra width, and efficiency. The higher the peak for these samples is, the lower are their PCE, V_{OC}, and I_{SC}.

However, the same inverse relation was not displayed for dyes that did not contain chlorophyll and consisted of different pigment(s). Wider absorption spectra and higher peak, intensity result in high V_{OC}, I_{SC} and PCE. This relationship can be observed in previous literature for chemically synthesised dyes like N719, as well as for natural dye extracts from the likes of mangosteen, blackberry, jamun, and black plum, which did not contain chlorophyll pigments [37].

Although all natural dyes showed similar results in the absorption spectrum, sample M still output a relatively better PCE and fill factor compared to the other natural dyes. This can likely be explained as the reason for anthocyanin pigments having carbonyl and hydroxyl groups that provide anchoring between the pigment molecule and the TiO_2 structure [38]. While chlorophyll pigments, present in samples T, C, and S, lack these bonding sites and form weak Van der Waal bonds with the mesoporous TiO_2 layer [39]. In terms of stability, anthocyanin dyes have been reported to have relatively high stability compared to other natural pigments [40].

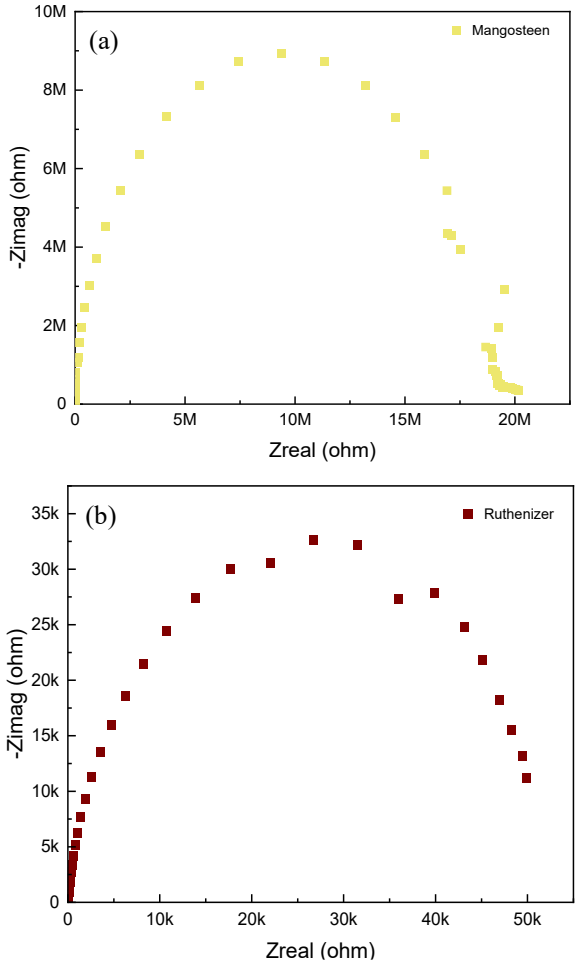

Fig. 7. (a) Nyquist plot for mangosteen dye DSSC, (b) Nyquist plot for Ruthenium dye DSSC.

Among the natural sensitisers tested, the best-performing dye sample was chosen and further evaluated against the control synthetic sensitiser. Figure 7 shows the Nyquist plots for DSSC based on the mangosteen dye and Ruthenizer dye, respectively.

A typical Nyquist plot often displays two to three semicircles associated with the frequency regions. Charge transfer resistance between the electrode and the electrolyte is often linked with the semicircle at the high-frequency region. While the charge transfer resistance at the interface between the dye and the electrolyte is usually attributed to the middle frequency region. The electrolyte charge resistance is associated with the low-frequency region [41, 42]. The higher impedance semicircles portrayed by sample M, compared to that for Ru dye, explain the higher photovoltaic performance of Ru in comparison to M. The radius of the M sample impedance is a few times higher than that of Ru. Large resistance is an indication of lower charge recombination [33].

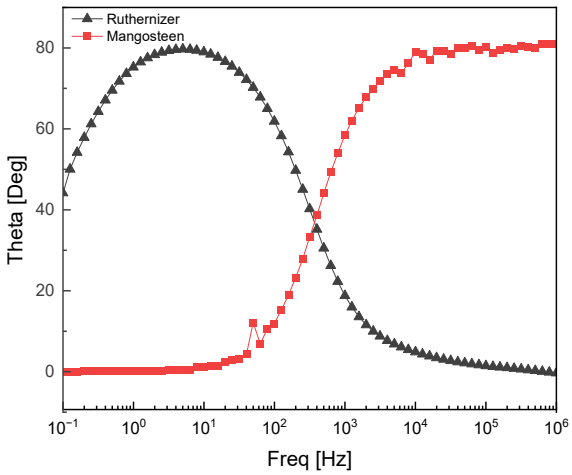

Fig. 8. Bode plot of DSSC fabricated with Ruthenium dye and mangosteen dye.

The Bode plot in Fig. 7 demonstrates Ru depicts a peak at low frequencies, while M exhibits a peak at comparatively higher frequencies. The Bode plot relates frequency to the lifespan of charge generated in the DSSC, as expressed in Eq. (4).

$$\tau = 1/(2\pi f) \quad (4)$$

A lower peak frequency means a higher lifespan for generated charge, and a longer lifetime of electrons is favourable for DSSC performance [43]. The longer electrons can exist before recombining means more electrons will have a higher chance of being transported to subsequent layers in the device structure and finally through the external circuit and back (via cathode) to form a complete circuit. Hence, Ru was seen to have better performance than M.

IV. CONCLUSION

Natural DSSC sensitisers were successfully extracted and benchmarked against those of commercial synthetic metal compound sensitisers; however, the dye extracted from mangosteen outperformed all the other natural sensitisers by achieving a PCE of 0.7%. The control sample using Ruthenizer sensitiser achieved a PCE of 3.9%. Coriander dye showed a decent performance with a PCE of 0.2%. Mangosteen dye performed better due to the presence of anthocyanin pigments, which are known to perform better in light harvesting than chlorophyll pigments, present in the coriander dye. Raw chlorophyll is unstable and does not offer proper binding sites in contrast to anthocyanin molecules. Anthocyanin molecules perform better and are more stable in acidic conditions. Future studies into these natural sensitisers with improvements, such as varying

pH levels or adding anchoring compounds/co-absorbents, are encouraged.

ACKNOWLEDGEMENT

The authors would like to acknowledge the financial sponsorship from Telekom Research and Development (TM R&D) Sdn. Bhd., under TM R&D Research Fund (Grant No: RDTC/231080, Project ID: MMUE/230009).

REFERENCES

[1] "CO_2 Emissions in 2022 – Analysis - IEA.", [Available online on 29 March 2025] https://www.iea.org/reports/co2-emissions-in-2022.

[2] S. Safieddine *et al.*, "Antarctic Ozone Enhancement During the 2019 Sudden Stratospheric Warming Event," *Geophys. Res. Let.t*, vol. 47, no. 14, pp. e2020GL0878102020.

[3] I. Wohltmann *et al.*, "Near-Complete Local Reduction of Arctic Stratospheric Ozone by Severe Chemical Loss in Spring 2020," *Geophys. Res. Lett.*, vol. 47, no. 20, pp. e2020GL089547, 2020.

[4] "What is the current state of the ozone layer? — European Environment Agency," [Available online on 29 March 2025] https://www.eea.europa.eu/themes/climate/ozone-depleting-substances-and-climate-change-1/protecting-the-ozone-layer-while.

[5] "Monthly Climate Reports | Global Climate Report | Annual 2024 | National Centers for Environmental Information (NCEI)," [Available online on 02 February 2025] https://www.ncei.noaa.gov/access/monitoring/monthly-report/global/202413.

[6] S. C. Lim, M. M. F. Dawoud, Y. H. Kwok and W. Y. Wong, "Recent Progress in Floating Solar Photovoltaic Systems: A Review from Malaysia's Perspective," *J. Eng. Technol. and Appl. Phys.,* vol. 6, no. 1, pp. 1–5, 2024.

[7] S. M. Sultan and M. N. Ervina Efzan, "Review on Recent Photovoltaic/Thermal (PV/T) Technology Advances and Applications," *Solar Ener.,* vol. 173, pp. 939-954, 2018.

[8] M. Benghanem *et al.*, "Evaluation of the Performance of Polycrystalline and Monocrystalline PV Technologies in a Hot and Arid Region: An Experimental Analysis," *Sustainability*, vol. 15, no. 20, pp. 14831, 2023.

[9] F. Mohamed Rosly, G. L. Ong, T. S. Ong, C. H. Nee, S. A. Ibrahim and S. S. Yap, "Simulation and Fabrication of P3HT:PCBM Solar Cell," *J. Eng. Technol. and Appl. Phys.*, vol. 5, no. 2, pp. 5–8, 2023.

[10] R. Wan *et al.*, "Investigation on Thermally Evaporated Aluminium Contact Layers for Perovskite Solar Cell Applications," *Int. J. Integr. Eng.*, vol. 16, no. 3, pp. 28–35, 2024.

[11] H. A. Fetouh, A. E. Dissouky, H. A. Salem, M. Fathy, B. Anis and A. E. Hady Kashyout, "Synthesis, Characterization and Evaluation of New Alternative Ruthenium Complex for Dye Sensitized Solar Cells," *Sci. Rep. 2024*, vol. 14, no. 1, pp. 1–13, 2024.

[12] S. Maw, "Performances Analysis and Comparison of Active and Hybrid Harmonic Filter in Photovoltaic Water Pumping System," *J. Eng. Technol. and Appl. Phys.,* vol. 5, no. 2, pp. 58–63, 2023.

[13] I. Yahaya and A. N. Rosli, "A Flash Flood Warning System Using Solar Powered Node MCU," *J. Eng. Technol. and Appl. Phys.*, vol. 7, no. 1, pp. 45–49, 2025.

[14] M. Grätzel, "Highly Efficient Nanocrystalline Photovoltaic Devices," *Platin. Met. Rev.*, vol. 38, no. 4, pp. 151 – 159, 1994.

[15] M. A. M. Al-Alwani, A. B. Mohamad, N. A. Ludin, A. A. H. Kadhum and K. Sopian, "Dye-Sensitised Solar Cells: Development, Structure, Operation Principles, Electron Kinetics, Characterisation, Synthesis Materials and Natural Photosensitisers," *Renew. and Sustain. Ener. Rev.,* vol. 65, pp. 183-213, 2016.

[16] C. Z. Eldjilali *et al.*, "Electrochromic Performances of Tio_2 Nanocrystals Thin Films for Smart Glass Applications," *Thin Solid Films*, vol. 815, pp. 140636, 2025.

[17] A. Aslam *et al.*, "Dye-Sensitized Solar Cells (DSSCs) as A Potential Photovoltaic Technology for The Self-Powered Internet of Things (IoTs) Applications," *Solar Ener.*, vol. 207, pp. 874-892, 2020.

[18] A. Roy, A. Ghosh, S. Bhandari, P. Selvaraj, S. Sundaram and T. K. Mallick, "Color Comfort Evaluation of Dye-Sensitized Solar Cell (DSSC) Based Building-Integrated Photovoltaic (BIPV) Glazing after 2 Years of Ambient Exposure," *J. Phys. Chem. C*, vol. 123, no. 39, pp. 23834–23837, 2019.

[19] M. Szindler, M. Szindler, A. Drygała, K. Lukaszkowicz, P. Kaim and R. Pietruszka, "Dye-Sensitized Solar Cell for Building-Integrated Photovoltaic (BIPV) Applications," *Materials*, vol. 14, no. 13, pp. 3743, 2021.

[20] N. I. M. Nawawi, G. Ijod, F. Abas, N. S. Ramli, N. Mohd Adzahan and E. Mohamad Azman, "Influence of Different Drying Methods on Anthocyanins Composition and Antioxidant Activities of Mangosteen (Garcinia mangostana L.) Pericarps and LC-MS Analysis of the Active Extract," *Foods*, vol. 12, no. 12, pp. 2351, 2023.

[21] S. Roseline, A. Yadav, B. Monteiro and F. S. Josephine, "Analysing The Various Pigments Present in Coloured Leaves", DOI: 10.13140/RG.2.2.15304.33287.

[22] A. Ali, P. Santoro, J. Mori, A. Ferrante and G. Cocetta, "Effect Of UV-B Elicitation on Spearmint's (Mentha spicata L.) Morpho-Physiological Traits and Secondary Metabolites Production," *Plant. Growth Regul.*, vol. 104, no. 1, pp. 63–76, 2023.

[23] J. M. El-Qudah, "Contents of Chlorophyll and Carotenoid Pigments In Common Thyme (Thymus vulgaris L.)," *World Appl. Sci. J.*, vol. 29, no. 10, pp. 1277–1281, 2014.

[24] Y. Iijima and A. Joh, "Pigment Composition Responsible for the Pale Yellow Color of Ginger (Zingiber officinale) Rhizomes," *Food Sci. Technol. Res.*, vol. 20, no. 5, pp. 971–978, 2014.

[25] Y. H. Shen *et al.*, "Exploring the Differential Mechanisms of Carotenoid Biosynthesis in The Yellow Peel and Red Flesh of Papaya," *BMC Genomics*, vol. 20, pp. 40, 2019.

[26] "Solaronix - Ruthenizer, Ruthenium Photo-Sensitizers,": [Available online on 29 March 2025] https://www.solaronix.com/materials/products/ruthenizer/.

[27] M. E. Yeoh and K. Y. Chan, "Synthesis of Dye-sensitised Solar Cells Utilising Platinised Counter Electrode," *Mater. Res. Innov.*, vol. 21, no. 4, pp. 244–248, 2017.

[28] M. E. Yeoh, K. Y. Chan and H. Y. Wong, "Investigation on The Thickness Effect of TiO_2 Photo-Anode on Dye-Sensitized Solar Cell Performance," *Solid State Phenomena*, vol. 280, pp. 76–80, 2018.

[29] Z. Yu, N. Vlachopoulos, M. Gorlov and L. Kloo, "Liquid Electrolytes for Dye-Sensitized Solar Cells," *Dalton Trans.*, vol. 40, no. 40, pp. 10289–10303, 2011.

[30] N. H. Astuti, N. A. Wibowo and M. R. S. S. N. Ayub, "The Porosity Calculation of Various Types of Paper Using Image Analysis," *Jurnal Pendidikan Fisika Indonesia*, vol. 14, no. 1, pp. 46–51, 2018.

[31] W. Li, R. Liang, A. Hu, Z. Huang and Y. N. Zhou, "Generation of Oxygen Vacancies in Visible Light Activated One-Dimensional Iodine TiO_2 Photocatalysts," *RSC Adv.*, vol. 4, no. 70, pp. 36959–36966, 2014.

[32] M. E. Yeoh *et al.*, "A Novel Simplified Approach in Fabricating TiO_2 Photoanodes for Dye-Sensitized Solar Cells," *Mater. Lett.*, vol. 349, pp. 134730, 2023.

[33] L. Sun, "Asphalt Mix Homogeneity," *Structural Behavior of Asphalt Pavements*, Elsevier Inc., pp. 821–921, 2016.

[34] M. Ryan, "Progress in Ruthenium Complexes for Dye Sensitised Solar Cells," *Platin. Met. Rev.*, vol. 53, no. 4, pp. 216 – 218, 2009.

[35] N. Sofyan, A. Ridhova, A. H. Yuwono and A. Udhiarto, "Fabrication of Solar Cells with TiO_2 Nanoparticles Sensitized using Natural Dye Extracted from Mangosteen Pericarps," *Int. J. Technol.*, vol. 8, no. 7, pp. 1229-1238, 2017.

[36] G. Calogero, J. H. Yum, A. Sinopoli, G. Di Marco, M. Grätzel and M. K. Nazeeruddin, "Anthocyanins and Betalains As Light-Harvesting Pigments for Dye-Sensitized Solar Cells," *Solar Ener.*, vol. 86, no. 5, pp. 1563-1575, 2012.

[37] A. Sikder *et al.*, "Characterization and Comparison of DSSCs Fabricated with Black Natural Dyes Extracted from Jamun, Black Plum, and Blackberry," *Energies*, vol. 16, no. 20, pp. 7187, 2023.

[38] W. Ghann *et al.*, "Fabrication, Optimization and Characterization of Natural Dye Sensitized Solar Cell," *Sci. Rep.*, vol. 7, pp. 41470, 2017.

[39] W. A. Ayalew and D. W. Ayele, "Dye-Sensitized Solar Cells Using Natural Dye as Light-Harvesting Materials Extracted from Acanthus Sennii Chiovenda Flower and Euphorbia Cotinifolia Leaf," *J. Sci.: Adv. Mater. and Device.*, vol. 1, no. 4, pp. 488-494, 2016.

[40] E. M. Abdou, H. S. Hafez, E. Bakir and M. S. A. Abdel-Mottaleb, "Photostability of Low Cost Dye-sensitized Solar Cells Based on Natural and Synthetic Dyes," *Spectrochim. Acta A Mol. Biomol. Spectrosc.*, vol. 115, pp. 202–207, 2013.

[41] S. Sarker, A. J. S. Ahammad, H. W. Seo and D. M. Kim, "Electrochemical Impedance Spectra of Dye-Sensitized Solar Cells: Fundamentals and Spreadsheet Calculation," *Int. J. Photoenergy*, vol. 2014, no. 1, pp. 851705, 2014.

[42] A. M. Ammar, H. S. H. Mohamed, M. M. K. Yousef, G. M. Abdel-Hafez, A. S. Hassanien and A. S. G. Khalil, "Dye-Sensitized Solar Cells (DSSCs) Based on Extracted Natural Dyes," *J. Nanomater*, vol. 2019, no. 1, pp. 1867271, 2019.

[43] A. Omar, M. S. Ali and N. Abd Rahim, "Electron Transport Properties Analysis of Titanium Dioxide Dye-Sensitized Solar Cells (TiO_2-DSSCs) based Natural Dyes Using Electrochemical Impedance Spectroscopy Concept: A Review," *Solar Ener.,* vol. 207, pp. 1088-1121, 2020.